Collapse of dry and immersed polydisperse granular columns: A unified runout description

Oscar Polanía *
LMGC, Université de Montpellier, CNRS, Montpellier, France
and Department of Civil and Environmental Engineering,Universidad de los Andes, Bogotá, Colombia

Miguel Cabrera
Department of Civil and Environmental Engineering,Universidad de los Andes, Bogotá, Colombia

Mathieu Renouf
LMGC, Université de Montpellier, CNRS, Montpellier, France

Emilien Azéma
LMGC, Université de Montpellier, CNRS, Montpellier, France
and Institut Universitaire de France (IUF), Paris, France

(Received 6 December 2021; accepted 27 July 2022; published 22 August 2022)

The granular column collapse is a simplified version of granular flows such as landslides, avalanches, and other industrial processes mobilized in air or within a fluid. In this configuration, the particles collapse in an accelerating phase, reaching a state of constant spreading velocity until they decelerate and stop. Granular flows commonly involve particles of different sizes, a property termed polydispersity. Understanding the role of polydispersity remains a challenging task that is often analyzed with nearly monodisperse systems and demanding a series of simplifications when coupled with a fluid in a numerical model. Here, we study the effect of particle-size polydispersity in dry and immersed granular columns, using a finite element method-discrete element method model for fluid-particle interactions. We show that the velocity of the column collapse and runout distance decrease with an increase in the level of polydispersity in immersed conditions, and remain nearly independent of the level of polydispersity in dry conditions. Moreover, we find that the runout scales with the spreading front kinetic energy, weighted by the ratio between the particles' density and the density difference between particles and fluid. This scaling helps in identifying the governing processes in polydisperse granular columns, unifying the runout description of both dry and immersed collapses, and indicating that the column initial packing fraction is the governing parameter.

DOI: 10.1103/PhysRevFluids.7.084304

I. INTRODUCTION

Granular flows are found across scales, from geophysical mass flows such as landslides, debris flows, and pyroclastic flows, to industrial processes such as in pharmaceutic, cosmetic, and construction industries. In a granular system, the ratio between the particles volume V_p and a reference total volume V_t is known as the packing fraction $\phi = V_p/V_t$. For monodisperse particles, reference

*oscar.polania@umontpellier.fr, os.polaniao@uniandes.edu.co

values of ϕ are the random loose packing ($\phi_l = 0.55$) and random close packing ($\phi_c = 0.64$) [1]. Among granular flows, the presence of particles of different sizes, a property termed polydispersity, is a common characteristic. In a given granular system, ϕ grows with the level of polydispersity, because small particles fill the voids between coarse particles, resulting in an increase of the system bulk density [2]. Furthermore, granular flows occur in varied ambient fluids (e.g., air, water) where particle-fluid interactions significantly influence their behavior (e.g., collapse sequence, front velocity, final deposit), balancing the forces associated to the collective particles inertia and the ambient fluid viscosity. Courrech du Pont *et al.* [3] propose three flow regimes as a function of the Stokes number $\mathrm{St} = (\rho_p \Delta\rho g d^3)^{1/2}/(18\mu_f\sqrt{2})$ and the density ratio $\chi = \sqrt{\rho_p/\rho_f}$, where d is the particle diameter, g is the gravitational acceleration, μ_f is the fluid dynamic viscosity, ρ_p and ρ_f are the particle and fluid densities, respectively, and $\Delta\rho = \rho_p - \rho_f$ is the density difference between particles and fluid. The three flow regimes and the limits between them are the free-fall regime where ambient drag is negligible. This regime occurs for $\mathrm{St} \geqslant \mathrm{St}^*$ and $\chi \geqslant \chi^*$, where $\mathrm{St}^* = 10$ and $\chi^* = 4$ are the transition limits to the inertial and viscous regimes. The inertial regime occurs when particle-particle and particle-fluid drag interactions are strong, occurring for any pair of St and χ below their transition values and for a ratio $\mathrm{St}/\chi > 2.5$. The viscous regime occurs when particles are limited by their Stokes velocity, and for $\mathrm{St}/\chi < 2.5$.

A benchmark configuration in the study of granular flows is the collapse of a granular column. On it, a granular assembly is built with an initial height H_0 and an initial length L_0, resulting in an aspect ratio $A = H_0/L_0$. The column collapses by self-weight over a horizontal plane, leaving a final deposit with height H_f and runout L_f. The collapse sequence begins with a vertical fall of particles. Then the column starts a horizontal acceleration phase, reaching a state of constant spreading velocity until it decelerates and stops. For short columns, identified with $A < 2.3$ in two-dimensional simulations [4], the free fall only occurs for particles at the column free face.

The relationship between the column mobility and its aspect ratio is found in experimental dry [5,6] and immersed cases [7–9], and in numerical dry [4,10] and immersed simulations [11–14], showing how L_f varies with A in the aforementioned flow regimes. Besides the influence of A, the column mobility is linked to the collapse kinematics [10]. Numerically, previous studies link the column mobility with the peak kinetic energy of a single grain in dry and immersed cases [11]. Other studies show that L_f scales linearly as a function of the front velocity during steady state U, a characteristic flow height (e.g., H_0), the ratio between ρ_f and ρ_p, and g [15,16]. Moreover, the column final runout L_f is a descriptor of the deposit shape, which is a macrorepresentation of the friction coefficient between particles [17]. For dry granular columns, the final runout is found to be independent of the column polydispersity [18], confirming the observations on simple shear cells and proving an nonexistent effect of polydispersity on the macroscopic friction angle [19–22].

Previous studies on immersed granular flows show that increasing ϕ enhances, for example, the effective viscosity [23]. In consequence, in immersed monodisperse columns, the collapse sequence depends on the column initial packing fraction ϕ_0, where initially loose columns collapse faster and reach longer runouts than dense columns [24,25]. Despite the agreement of the column density influence on the final runout in monodisperse columns, the relationship with ϕ_0 remains to be confirmed in highly polydisperse columns, where only few experimental studies have explored the collapse of a bidisperse granular system [26,27].

In this study, we are interested in the collapse of granular columns with different particle-size distributions (PSD) in dry and immersed conditions. We focus on clarifying the role of polydispersity on the column collapse sequence and final runout. We aim to extend the observations on monodisperse column collapses, in both dry and immersed conditions, to polydisperse columns by exploring a wide range of PSDs, ranging from relative initially loose to initially dense packings. We employ a finite element method (FEM) coupled with a contact dynamics discrete element method (DEM), for the fluid and solid phases, respectively. The simulation of such systems is computationally expensive due to the large number of particles required for representative granular samples, the necessary short computation time step for avoiding particle interpenetrations on the smallest particles, and the challenging coupling of the momentum transfer from a moving particle

cluster to the fluid mesh. These challenges are successfully managed in the simulation campaign, guaranteeing that there is no penetration during the contact solution in the nonsmooth DEM and employing a fluid solution that can manage high packing fractions, resulting in the computation of particle-fluid interactions that are not precise.

The paper is organized as follows. The numerical methods, and the description of the simulation campaign are presented in Sec. II. The characteristics of the column collapse are described in Sec. III. The collapse kinematics and the column final runout are discussed in Secs. IV and V, respectively. In Sec. VI we propose a scaling between the final runout and the collapse energy; and finally, conclusions are presented in Sec. VII.

II. METHODS

A. Coupled FEM-DEM model

As mentioned above, the current study is conducted in a coupled finite element method (FEM) with a discrete element method (DEM), simulating the collapse of a granular column in different ambient fluids. For the fluid motion, we employ a continuous representation solved with a finite element spatial discretization combined with an implicit temporal discretization of the incompressible Navier-Stokes equations [28]. The method couples the particle discrete solution with the fluid continuum solution by a loop solver that first obtains the packing fraction within each mesh element and then computes the resultant fluid velocity, fluid pressure, and particles-fluid interaction forces with the current state variables, which are the fluid velocity, the fluid pressure, and the particles' velocity. Particles-fluid interactions forces considered in the model are buoyancy and drag [see Eqs. (A1) and (A4) in the Appendix]. The drag model formulation for a single particle takes into account the influence of the surrounding particles with a function of ϕ [see Eq. (A5)], found to be satisfactory for ϕ above the random loose packing ϕ_l [29]. A drag model formulation for polydisperse and highly dense granular flows remains an open question. Although alternative methods to compute the drag force in polydisperse systems have been recently formulated [30–32], the model employed in this work accounts for the polydispersity level by associating it to an increase in packing fraction, relative to a monodisperse PSD. Moreover, in this framework the hydrodynamic torque is assumed to be zero and no lubrication forces are considered between particles.

The coupled computation results in the particle source terms for the next time step of the DEM computation, updating the particle position. In this approach, a coupled coarse-scale solution is an appealing approximation for the fluid motion, being capable of managing polydisperse systems with high packing fractions, and demanding special care in the mesh sizing relative to the maximum particle diameter.

The granular system is simulated with the nonsmooth contact dynamics approach (NSCD) developed by Moreau and Jean [33,34]. The method is a class of the DEM, where perfectly rigid bodies interact by volume exclusion and Coulomb friction. In this method, the equations of motion are integrated in a time step obtaining the particles kinematics. This method is convenient for the simulation of highly polydisperse systems, because volume exclusion allows a complete interaction between small and big particles without the need of tailored stiffness parameters as in the smooth DEM class. Also, the method employs a stable integration scheme without the need of stabilization techniques [35].

In this study, we use, out of simplicity, two open-source software packagesfor the simulation of the granular column collapse. LMGC90 [36] is used for dry granular columns and MIGFLOW [37] is used for immersed granular columns. Both software packages employ equivalent formulations of the DEM. We have made the necessary tests to justify the implementation of both codes, resulting in equivalent macroscopic behaviors. For faster simulations, we use parallel computing available in LMGC90 and use PETSC4PY package [38] for solving the fluid motion equations in MIGFLOW.

An immersed granular column collapse is intrinsically a three-dimensional process, allowing fluid percolation through the moving granular media in all directions. In our simulations, the

granular domain is simplified into a two-dimensional representation, where fluid percolation is obstructed by a large packing fraction, larger than in a three-dimensional system. An alternative for solving the particle-fluid interaction, representing the three-dimensional packing fraction within a two-dimensional system, is to reduce the particle's diameter, seen by the fluid phase, by an *ad hoc* factor. Kumar *et al.*, employing a different framework with a DEM coupled with a lattice Boltzmann method, use a factor of 0.9 to model the permeability of a three-dimensional case with a two-dimensional approach [39]. In this work, we opt for a similar solution reducing all particle diameters by a factor of 0.9 for representing a three-dimensional packing fraction in a two-dimensional simulation domain when computing the particle-fluid interactions.

Finally, we use a constant fluid mesh element size, computing the particle-fluid interaction as a function of the packing fraction. Potential limitations of this approach can be related to the size ratio between the fluid elements and the smallest particles in the system, oversimplifying the momentum transfer between fluid and small particles. However, we focus on the macroscopic effects that polydispersity has on the column collapse controlled by the packing fraction and not by the calculation of the motion of single particles, resulting in a cost-effective numerical framework. Other approaches, such as the one of Capecelatro and Desjardins [40], could be employed to model polydisperse systems and provide a more detailed solution at the particle scale, demanding a higher computational cost.

B. Column construction and collapse

The columns studied in this work consist of a two-dimensional granular system of variable levels of polydispersity, defined by the particle-size ratio $\lambda = d_{\max}/d_{\min}$, relating the size of the biggest to the smallest particle. In our simulations, we study five values of $\lambda = [1.2, 3, 5, 10, 19]$. For all values of λ, we use a PSD that consists of 25 disk diameters, linearly distributed between $d_{\min}$ and $d_{\max}$. In all the resultant PSDs, the number of particles per diameter is set to have the same mass. This means that each particle diameter has $1/25$ of the mass necessary for filling the initial column dimensions. For all PSDs, the particle diameter $d_{50} = 0.001$ m has a cumulative unitary mass, relative to the column total mass, of 0.5. The minimum and maximum diameter are equal to $d_{\min} = 2d_{50}/(\lambda + 1)$ and $d_{\max} = d_{\min}\lambda$, respectively. The median diameter $\overline{d}$ ranges between [0.0001 : 0.001] m [see Figs. 1(a) and 1(b)]. The disks have $\rho_p = 1500\,\mathrm{kg/m^3}$, with a friction coefficient of 0.3, typically encountered in geomaterials [41], and restitution coefficient of 0 found not to affect the collapse behavior of granular columns [17].

The columns initial length L_0 is equal to 0.05 m, and the initial height H_0 varies between [0.015 : 0.25] m, covering seven column aspect ratios $A = [0.3, 0.5, 0.75, 1.0, 2.0, 3.5, 5.0]$ and allowing the study of short and tall columns. Cabrera and Estrada show that particle-size effects become negligible in the column final runout when the ratio between L_0 and the average particle diameter $\langle d \rangle$ is at least 50 [4]. In this work, we fulfill this condition in all cases, considering $\langle d \rangle$ as d_{50} or $\overline{d}$. Moreover, the total number of particles N_p in each column varies with A and λ, ranging between $N_p \approx [1000 : 110000]$.

The columns are built as an initial gravity deposit of particles in a rectangle with dimensions L_0 and H_0, and are let to settle by self-weight. The columns have an initial packing fraction ϕ_0, varying between loose to very dense packings relative to the random loose ϕ_l and random close packing ϕ_c for monodisperse disks [42,43] [see Fig. 1(c)]. The column collapse is set by removing the lateral wall and is driven by the particles' self-weight with $g = 9.81\ \mathrm{m/s^2}$. L_f and H_f describe the deposit geometry when the collapse finishes (see Fig. 2). We measure L_f as the position of the farthest particle with three active contacts still in touch with the deposit bulk. Three repetitions of each combination of λ and A are performed by randomly shuffling the particles location, resulting in a new gravity deposit and avoiding the effect of the initial particle spatial distribution within the column. In this work, a total of 189 simulations are performed. The time step was chosen relative to $d_{\min}$ and H_0 as $dt < d_{\min}/\sqrt{2H_0 g}$. For simplicity, we use $dt = 0.0001$ s and, for extreme cases with $A = [3.5, 5.0]$ and $\lambda = [10, 19]$, $dt = 0.00001$ s. Note that both dt values satisfy the inequality.

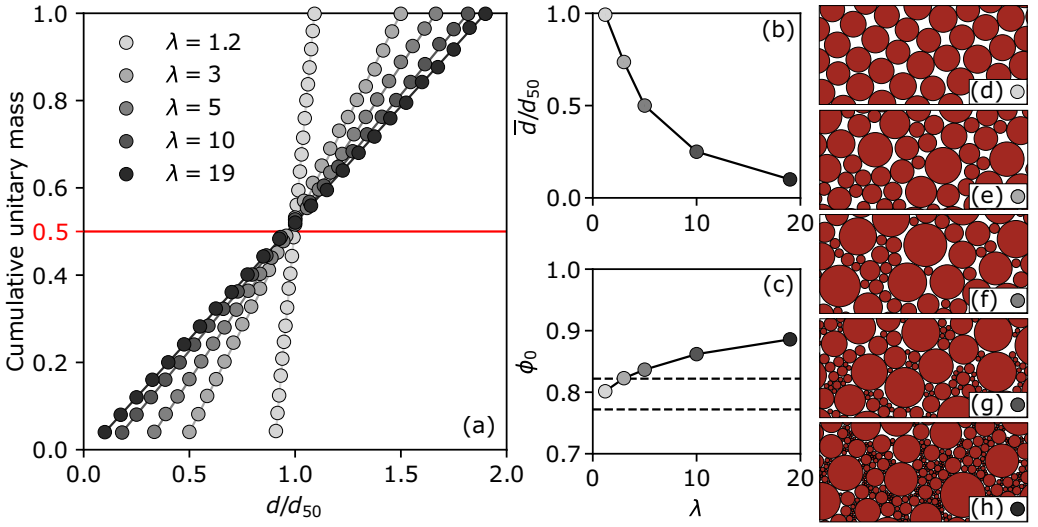

FIG. 1. (a) Particle size distribution as a function of the size ratio $\lambda = d_{\max}/d_{\min}$, with a common cumulative mass of 0.5 for $d_{50} = 0.001$ m. (b) Normalized median particle diameter $\overline{d}/d_{50}$ as a function of λ. (c) Initial packing fraction ϕ_0 as a function of λ, where the dashed lines indicate the random loose ($\phi_l = 0.772$) and random close packing ($\phi_c = 0.822$) for monodisperse disks [42,43]. (d)–(h) Close-up views show the polydispersity level for $\lambda = [1.2, 3, 5, 10, 19]$.

The fluid is solved in a rectangular domain composed of a regular mesh of triangular elements of size $5d_{50}$. The domain boundaries are considered as walls with no flux across them, and with pressure set to zero only at the upper wall. The mesh domain is found to be sufficiently large for avoiding pressure reflections at the foremost boundaries. The fluid has the properties of water with density $\rho_f = 1000$ kg/m^3 and viscosity $\mu_f = 0.001$ Pa s. Moreover, the physical parameters of particles and fluid that we use have been previously employed to validate the numerical framework approximation [28].

In this study, assuming the fluid density and viscosity as zero, the collapse of dry columns simulate flows in the free-fall regime with the Stokes number $\mathrm{St} \gg \mathrm{St}^*$ and $\chi \gg \chi^*$. Note that the "$*$" marks the transition limits presented by Ref. [3]. Within these regimes, immersed columns focus on flows that belong to the inertial regime with $\mathrm{St} = 3.37$ and $\chi = 1.22$, both considering the representative particle diameter as d_{50}. These values of St and χ allow the study of granular flows near the transition between inertial and viscous flows, relative to monodisperse systems, aiming at highlighting the role of the level of polydispersity in the collapse regimes. Our immersed simulations have $\mathrm{St}/\chi = 2.76$, a value that is close to the regime transition at $\mathrm{St}/\chi = 2.5$ [3]. In Sec. IV we refer to the relevance of studying polydisperse columns near this regime transition.

III. COLLAPSE SEQUENCE

During the collapse of a granular column, the particles in movement are separated from the motionless particles by a sliding or failure plane. In the sequence of dry column collapses, we observe the rapid development of this sliding plane that, regardless of the level of polydispersity, shows a similar inclination in columns with the same aspect ratio A at a similar collapse instant. This similarity in the collapse dynamics occurs from beginning to end of the collapse sequence, implying that the sliding plane is independent of λ [see Figs. 2(a) and 2(b)]. On the contrary, it becomes evident that polydispersity changes the collapse sequence of immersed collapses [see Figs. 2(c) and

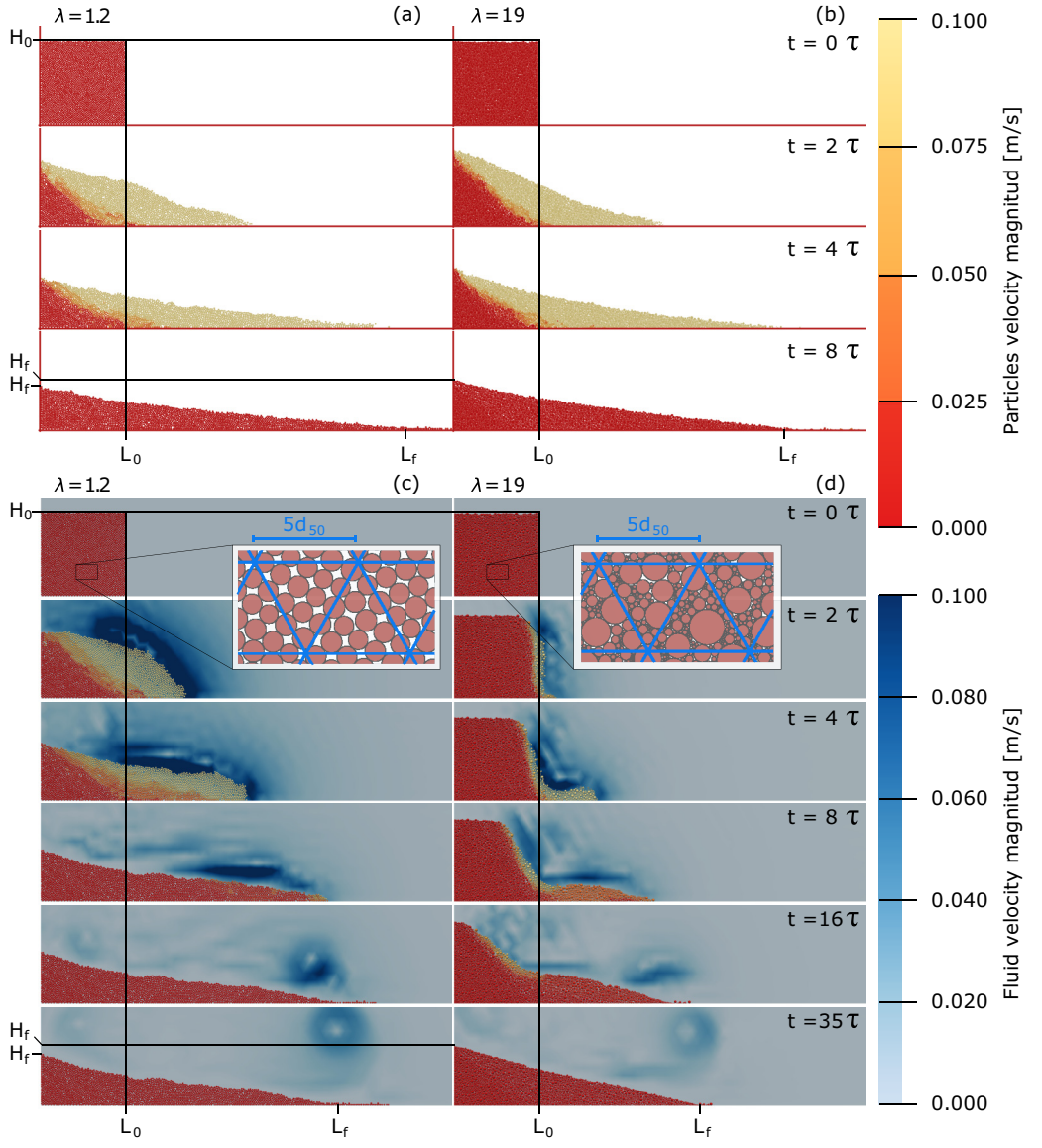

FIG. 2. (a), (b) Collapse sequence of dry and (c), (d) immersed columns. The columns have an aspect ratio $A = H_0/L_0 = 1.0$ and particle-size ratio $\lambda = [1.2, 19]$ (left, right). τ is a characteristic time $\tau = \sqrt{H_0/g^*}$, where g^* stands for a reduced gravity due to the ambient fluid buoyant force $g^* = g\,\Delta\rho/\rho_p$, and $\Delta\rho = \rho_\mathrm{p} - \rho_\mathrm{f}$ is the density difference between particles and fluid. The insets in (c) and (d) compare the particles size with the fluid mesh size.

2(d)]. Columns with low levels of polydispersity ($\lambda = 1.2$) rapidly develop an inclined sliding plane of a thick layer of moving particles, and at high levels of polydispersity ($\lambda = 19$) the sliding plane tends towards a thin and nearly vertical layer of moving particles, while most of the core remains nearly static. In the latter, the initial mobilization results in the free fall of particles at the column release face, slowly propagating inwards as a sequence of steep and thin slides (see Supplemental Material (movies) [44]). The inwards propagation of thin slides has been previously observed experimentally by Thompson and Huppert on the study of immersed sand column collapses,

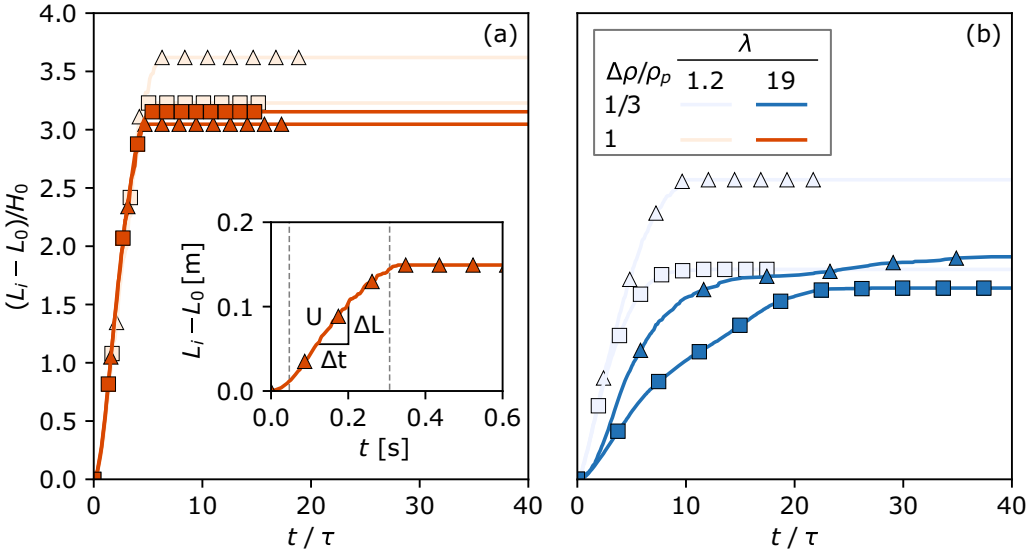

FIG. 3. Front position evolution L_i during collapse and relative to the column initial dimensions (L_0, H_0), for (a) dry and (b) immersed columns and for $A = [1.0, 3.5]$ (△,□), respectively, and $\lambda = [1.2, 19]$. The inset in (a) shows the evolution of L_i for $\lambda = 19$ and $A = 1.0$, and dashed gray lines delimit the collapse steady propagation stage interval.

suggesting that the occurrence of such behavior is caused by the particle angularity [45]. Here, we argue that an increase in λ leads to more stable columns, by means of denser packings [see Fig. 2(b)], frustrating the fluid percolation through the whole collapse sequence. In consequence, the frustrated percolation limits the amount of mobilized particles, leading to the formation of thin nearly vertical slides.

The column front translation provides simplified information on the entire collapse sequence, such as collapse velocity, collapse sequence stages, and column mobility. After the initiation of the column collapse, the front translation has a distinct initial stage of acceleration until reaching a steady side propagation. Later, the front decelerates and stops at the runout distance L_f. Figure 3 shows the instantaneous evolution of the front position L_i normalized by H_0, for a timeline scaled by a characteristic time $\tau = \sqrt{H_0/g^*}$, where g^* stands for a reduced gravity due to the ambient fluid buoyant force $g^* = g\Delta\rho/\rho_p$ [15]. Herein, the factor $\Delta\rho/\rho_p = 1/3$ and $\Delta\rho/\rho_p = 1$ stands for immersed and dry scenarios, respectively. During the steady propagation stage, dry column collapses share a common slope regardless of λ, while for immersed columns collapses, this only occurs at low levels of polydispersity ($\lambda < 5$), and the whole column collapse lasts longer with the increment of λ. The slope between L_i and t represents the front velocity U computed in the interval where the front propagation has a steady stage with no acceleration [see inset of Fig. 3(a)]. Moreover, L_f is consistently longer in dry columns than in immersed columns [see Fig. 3(b)]. The relationship between L_f, λ, A, and U is further discussed by means of a simplified model in Sec. VI. A table with the parameters of each simulation and the main results that support our study is included as Supplemental Material [44].

IV. FRONT KINEMATICS

From the previous observations, we can highlight that the level of polydispersity has a significant effect on the collapse sequence of immersed columns but a minimal effect on dry columns. As a result, highly polydisperse columns last longer in immersed conditions until coming to a full

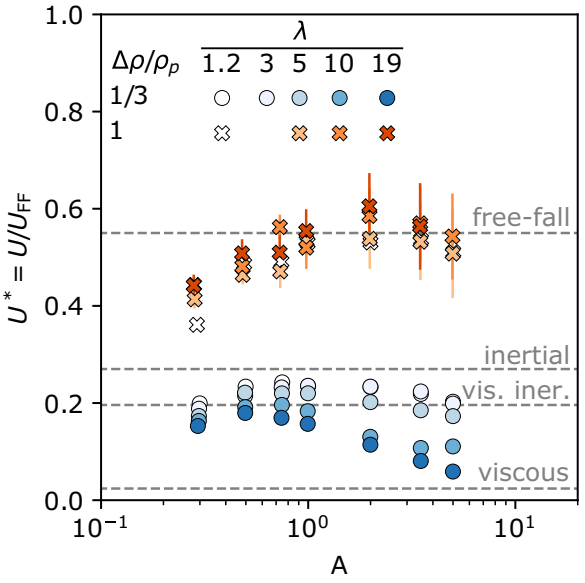

FIG. 4. Normalized front velocity U as a function of the column aspect ratio A. U_{FF} is the free-fall velocity $U_{\mathrm{FF}} = \sqrt{2H_0 g^*}$. The dashed lines are the characteristic velocities found by Bougouin and Lacaze for free-fall ($U^* \approx 0.55$), inertial ($U^* \approx 0.27$), viscous inertial ($U^* \approx 0.196$), and inertial regimes ($U^* \approx 0.024$) [9]. $\Delta\rho/\rho_{\mathrm{p}}$ is the density difference between particles and fluid $\Delta\rho = \rho_{\mathrm{p}} - \rho_{\mathrm{f}}$, and particles density ρ_{p}, where $\Delta\rho/\rho_{\mathrm{p}} = 1/3$ for immersed cases and $\Delta\rho/\rho_{\mathrm{p}} = 1$ for dry cases. Error bars correspond to the standard deviation of U between repetitions. Note that in immersed cases, the error bar is smaller than the marker size.

halt. Employing monodisperse particles, Bougouin and Lacaze [9] show that the collapse velocity in the steady state U is proportional to the free-fall velocity $U_{\mathrm{FF}} = \sqrt{2g^* H_0}$, with $U^* = U/U_{\mathrm{FF}} \approx [0.024, 0.196, 0.27, 0.55]$ for viscous, viscous inertial, inertial, and free-fall regimes, respectively. The common slope during the steady propagation stage for dry cases in Fig. 3(a) indicates that U is a function of H_0, confirming the proportionality proposed by Bougouin and Lacaze [9] and extending it to polydisperse systems in dry conditions. In our results, U fluctuates around a characteristic velocity of the free-fall regime ($U^* \approx 0.55$) in dry collapses. Those fluctuations are linked to the increment of λ, which overall leads to slightly faster collapses (see Fig. 4). Columns with $A < 1$ present lower values of U related to a shorter accelerating stage in its collapse sequence. Moreover, the normalized front velocity ranges between $U^* = [0.19 : 0.24]$ for immersed columns with $\lambda \leqslant 5$. This range is found to be characteristic of collapses between the viscous inertial and inertial regimes. An increment of λ reduces U^* in immersed cases, being more evident on columns with $A \geqslant 2$. This observation is notable and suggests that an increment in λ makes the collapse transition towards a viscous regime and an increment in the column aspect ratio A enhances this regime transition.

Under the assumption that U is the velocity resulting from the whole column mass M, we compute the kinetic energy during the steady propagation stage as $E_{\mathrm{K}}^{\mathrm{U}} = MU^2/2$, with $M = \sum_i^{N_p} m_i = \phi_0 \rho_{\mathrm{p}} H_0 L_0$, where m_i denotes the mass of each particle. At first glance, immersed collapses are less energetic than dry collapses. The energy of dry collapses increases with polydispersity because columns are denser and, contrary to immersed collapses, tend to be slightly faster. On both cases, $E_{\mathrm{K}}^{\mathrm{U}}$ grows as a function of A with a power law with an exponent of power index 2, regardless of the column level of polydispersity (see Fig. 5), while for immersed cases, this trend breaks at $\lambda > 5$. Note that, for immersed columns, the increment of λ consistently reduces E_K^U. Furthermore, the energy of tall ($A > 2$) and highly polydisperse columns ($\lambda \geqslant 10$) deviates from the quadratic tendency. This deviation of E_K^U coincides with the fact that the front velocity U transitions from the

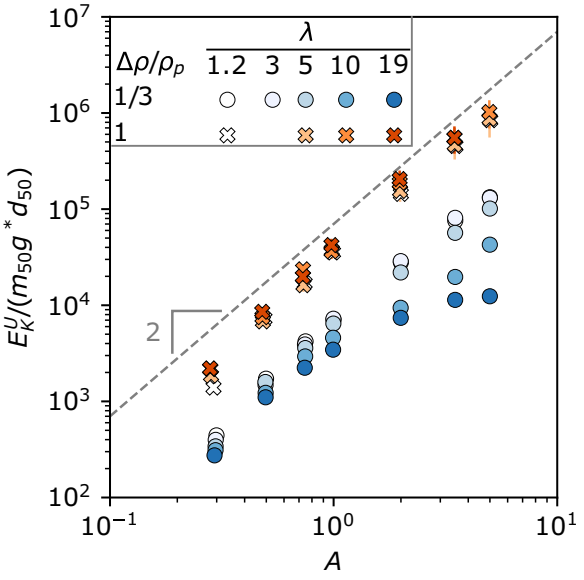

FIG. 5. Kinetic energy $E_K^U = MU^2/2$ during the steady propagation stage normalized by the characteristic energy of a single particle as a function of the column aspect ratio A. M is the column mass, d_{50} is a representative particle diameter, m_{50} is the mass of a single particle with diameter d_{50}, and g^* is the reduced gravity. Note that d_{50} and m_{50} are constant for all λ. Error bars correspond to the standard deviation of E_K^U between repetitions.

inertial to the viscous regime by the joined effect of the levels of polydispersity λ and the column aspect ratio A.

V. COLLAPSE MOBILITY

A common characteristic between dry and immersed columns is that the final runout increases with A and it follows a function in the form of a power law $L^* = A^\beta$, where $L^* = (L_f - L_0)/L_0$. Although the power law holds for polydisperse systems in dry and immersed cases [see Fig. 6(a)], the final runout L^* of immersed columns within an ambient fluid tends to shorten with polydispersity. L^* collapses on a power law with the exponent $\beta = 1$ for columns with $A < 2$. For taller columns $A \geqslant 2$, L^* deviates with $\beta = [0.92, 0.56]$ for dry and immersed cases, respectively, representing the transition from short to tall columns. The exponent $\beta = 1$ for short columns agrees with previous numerical studies [4,10,11]. For tall columns, the exponent $\beta = 0.92$ exceeds the common range $0.66 \leqslant \beta \leqslant 0.80$ [4,5,10], and for immersed collapses the result $\beta = 0.56$ is within the range $0.56 \leqslant \beta \leqslant 0.64$ [11,14].

An interesting remark is that L^* appears to be limited by the effect of λ for both dry and immersed columns, showing common values of L^* within the same A. This limited effect of λ on L^* is independent of the polydispersity level in dry columns, confirming previous works [18–21], and is seen in the immersed columns as a decrease of L^* when λ increases, saturating for $\lambda \geqslant 10$ [see Fig. 6(c)]. The reduction of the final runout in immersed cases suggests that the macroscopic friction angle depends on the level of polydispersity up to a given value of λ, here observed for $\lambda \leqslant 5$.

VI. SCALING: KINETICS AND RUNOUT

Based on the previous sections, we can make global observations for dry and immersed conditions relating the collapse energy and the column final runout. Dry columns are more energetic

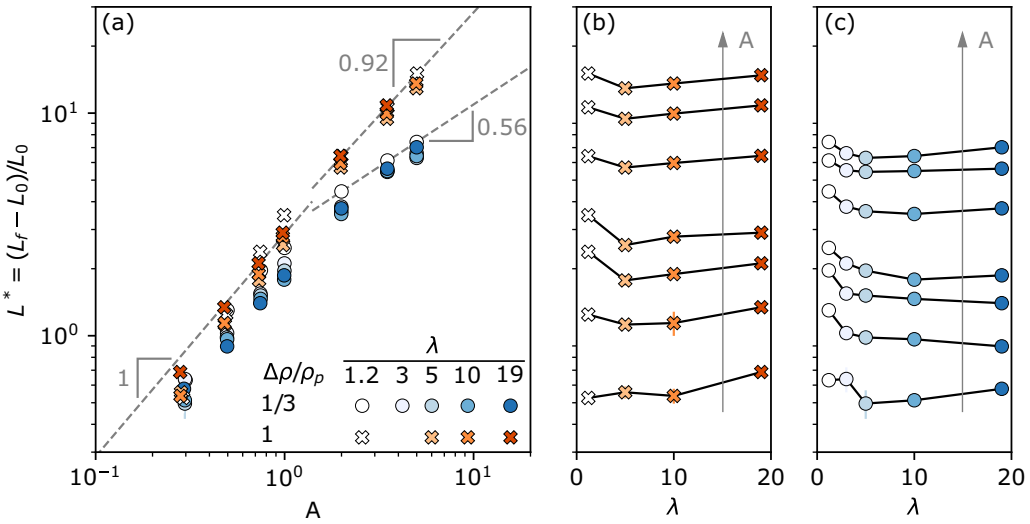

FIG. 6. (a) Normalized final runout L^* as a function of the column aspect ratio A, and as a function of the PSD size ratio λ for (b) dry and (c) immersed cases. The dashed lines in (a) are the best fits for a function in the form of $L^* = \alpha A^\beta$ for $\lambda = 1.2$ with the values of β shown in gray. L_0 is the initial column length, and L_f is the final runout. Error bars correspond to the standard deviation of L_f between repetitions.

and have a longer runout than immersed columns. In immersed columns, the energy decreases with the level of polydispersity, and the final runout tend to decrease with the increment of the polydispersity reaching a limit controlled by the macroscopic friction angle. Therefore, we propose a unified scaling for the processes involved in the column mobility and collapse kinematics for both dry and immersed cases.

Topin *et al.* propose a scaling with the analogy of a falling particle subjected to a viscous drag force [11]. In this study, we can not achieve such simplification because the particles' different sizes. Moreover, Lajeunesse *et al.* propose a force balance between the basal frictional force, as a function of the front velocity U, and an opposing force related to a reference wedge weight [5]. Here, we propose a similar simplified model with the analogy of a sliding block with an initial velocity and opposite resistance such that $M\ddot{x}(t) = -k\dot{x}(t)$, where $\dot{x}(t)$ and $\ddot{x}(t)$ are the block velocity and acceleration, respectively, and k is an equivalent suspension viscosity. Solving this equation, and considering the initial velocity as U and the initial position as L_0, we get at an infinite time:

$$L_f - L_0 = MU/k. \tag{1}$$

We divide both sides by L_0 and include E_K^U in Eq. (1), obtaining

$$L^* = \frac{\sqrt{2}}{kL_0}\sqrt{M}\sqrt{E_K^U}. \tag{2}$$

According to Eq. (2)

$$L^* \propto \sqrt{M}\sqrt{E_K^U}. \tag{3}$$

With these considerations the column final runout and the collapse kinematics of dry and immersed cases notably scale (see Fig. 7). Although dry and immersed configurations scale on different slopes, it is remarkable that the simplified model collapses for all levels of polydispersity.

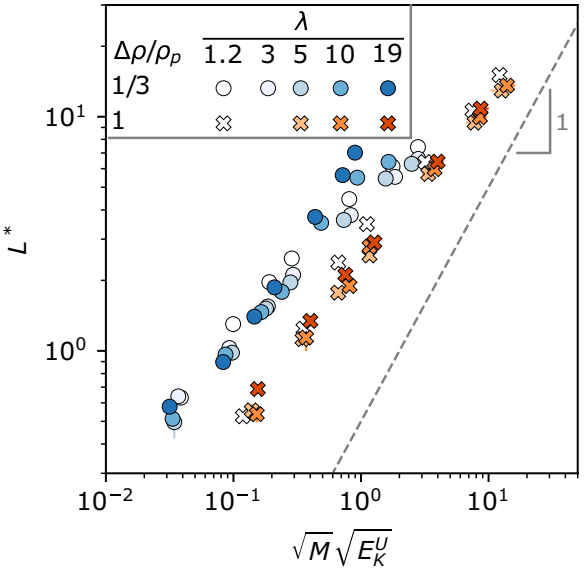

FIG. 7. Scaling of the normalized final runout L^* with the column kinematics according to Eq. (2). M is the column mass, and E_K^U is the kinetic energy. Error bars correspond to the standard deviation of L^* and E_K^U between repetitions.

An evaluation of the dependency of L^* with the model variables M and E_K^U shows a clear distinction in the trend for $M > 5$, that corresponds to columns with an aspect ratio $A \geqslant 2$. Note in Fig. 6(a) that the trend breaks for $A \geqslant 2$, distinguishing between short and tall columns. Consequently, M allows an alternative distinction between short and tall columns, considering that taller columns result in a larger amount of particles [see Fig. 8(a)]. As a function of E_K^U, there are two parallel trends that follow a power law with an exponent of power index 0.5 [see Fig. 8(b)], indicating that

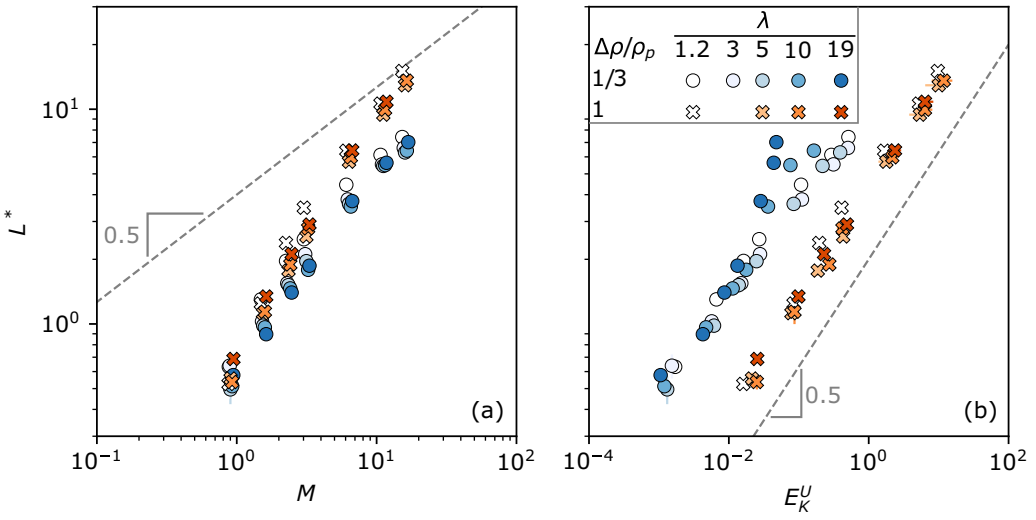

FIG. 8. Normalized runout L^* as a function of (a) the column mass M, and (b) the kinetic energy E_K^U during the steady propagation stage. Error bars correspond to the standard deviation of L^* and E_K^U between repetitions.

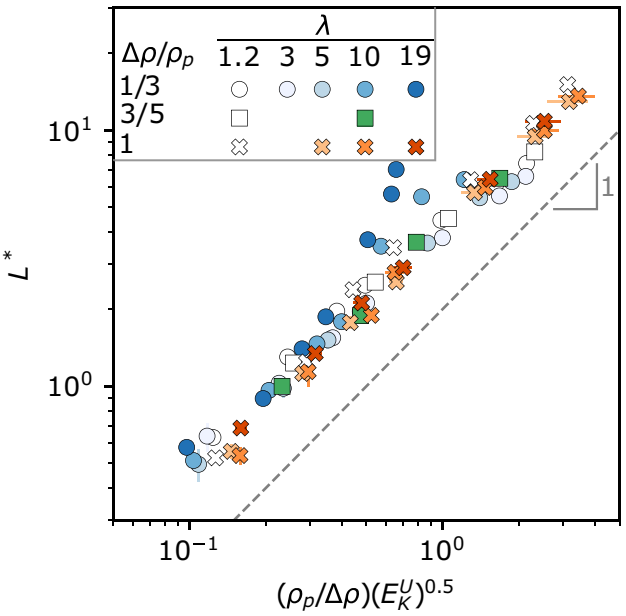

FIG. 9. Scaling of the normalized runout L^* with the column kinematics according to Eq. (4) with $(\delta, \epsilon, \zeta) = (0, 1, 0.5)$. ρ_p is the particles density, $\Delta\rho$ is the density difference between particles and fluid, and E_K^U is the kinetic energy during the steady propagation stage. Error bars correspond to the standard deviation of L^* and E_K^U between repetitions.

the energy difference of dry and immersed cases depends on a relation between the particles and the ambient fluid.

Based on the later observations, we include the column effective mass $M^* = M\Delta\rho/\rho_p$ in Eq. (3), and obtain:

$$L^* \propto (M^*)^{\delta}\left(\frac{\rho_p}{\Delta\rho}\right)^{\epsilon}\left(E_K^U\right)^{\zeta}, \tag{4}$$

where the exponents δ, ϵ, and ζ weigh the influence of each of the column controlling factors. The best scaling is obtained by setting $\delta = 0$, disregarding the distinction between short and tall columns, and setting $\zeta = 0.5$ and $\epsilon = 1$ resulting in a satisfactory scaling between E_K^U and L^* (see Fig. 9). Notably, all columns follow a common trend, despite the ambient fluid, the level of polydispersity, and the column aspect ratio. Deviations in the trend occur for immersed tall columns with $\lambda = 19$ when there are strong fluid effects (e.g., buoyancy and drag force), reducing the collapse velocity and implying a regime transition from inertial to viscous. Moreover, we include new simulations with $\rho_p = 2500$ kg/m^3 and $\Delta\rho/\rho_p = 3/5$, showing the reliability of the scaling and suggesting that the collapse is governed by a distinct combination of the factors $\Delta\rho/\rho_p$ and E_K^U. This scaling suggests, with the considerations mentioned above, that the column kinematics are directly related with the final runout, linking a faster collapse with a longer runout. Notably, the packing fraction ϕ_0, which increases with λ, can be suggested as a key parameter that governs the column kinematics, being stronger in immersed granular flows, and allows the characterization of the granular assembly by a characteristic grain diameter (e.g., $\langle d\rangle$, d_{50}, $\overline{d}$). This observation is in agreement with the observed relevance of ϕ_0 in immersed collapses [24], but extends it when ϕ_0 is larger than the monodisperse random close packing ϕ_c.

We acknowledge that the proposed scaling is an oversimplification of the entire physical problem. However, it is remarkable that this simple scaling captures the final runout and kinematics of a

granular column collapse when dry or immersed, and in a wide range of polydispersity levels. Notably, the scaling works well for the polydispersity levels that we employ, but deviates when fluid effects are strong. Although the level of polydispersity is not explicit in the scaling, it is essential in the computation of E_K^U, because the column bulk density varies with λ, and we evidence the dependency of the front velocity U to the level of polydispersity.

VII. CONCLUSIONS

We studied the collapse of granular columns in dry and immersed conditions with a coupled finite element method and discrete element method. We systematically varied the column aspect ratio, covering a range of short and tall columns while exploring different levels of polydispersity. Our results with monodisperse systems, for both dry and immersed conditions, are in agreement with previous experimental and numerical results. Moreover, we evidenced that the motion of immersed collapses is highly dependent on the level of polydispersity. We showed, in immersed columns, that the increment of the column polydispersity enhances the fluid-particles interactions, by increasing the column packing fraction and decreasing the front velocity and the column final runout. On the contrary, polydispersity does not have a strong effect on the collapse sequence and final runout of dry columns.

The increment in the polydispersity level reduces the final runout of immersed columns. However, we found that for high levels of polydispersity, the reduction of the final runout does not vary considerably. The principal effect of high levels of polydispersity is the change in the collapse sequence that results in slower front velocities, especially for tall columns, and a retrogressive thin sliding layer. Despite similar initial flow conditions between columns, relative to the Stokes number and the density ratio, there is evidence that an increase in the level of polydispersity results in the reduction of the front velocity, leading the column to transition from an inertial regime towards a viscous regime.

We propose a scaling that is an analogy of a simple sliding block model that has an initial velocity and an opposite resistance between the final runout and the front kinetic energy. In this scaling, and for immersed cases, we assume that the front carries all the viscous effects. Remarkably, the variables of the scaling can be easily measured in the laboratory and in numerical experiments. Moreover, this model suggests that, with the considerations mentioned above, the initial packing fraction is the governing factor of the column final runout and kinematics, allowing the characterization of the granular assembly by a characteristic grain diameter. Interestingly, we show that the scaling does not require a distinction of the involved mass, indicating that the final runout is only a function of the fluid-particles density ratio and the front kinetic energy. Regardless of its simplicity, it is notable that this simple scaling captures the final runout and kinematics of a granular column collapse when dry or immersed. Although the level of polydispersity is not explicit in the scaling, it is essential in the computation of the front kinetic energy, and we evidence the dependency of the front velocity to the level of polydispersity.

Finally, this work indicates that polydisperse immersed granular flows do not occur suddenly, rather they progressively slide over thin layers, as the level of polydispersity increases. These results show that highly polydisperse flows will last longer and develop slower flows. The practical implications of this model could be of great use in the hazard assessment of offshore infrastructure against submarine landslides or in the handling of immersed industrial granular systems such as fresh concrete, or in pharmaceutical and cosmetic applications.

Although our results are limited by the physical considerations that we have made, they agree with previous experimental and numerical results for monodisperse cases and contribute a perspective in the study of immersed polydisperse flows. Further studies could employ more precise physical assumptions, including lubrication to determine if it has a significant role on dense granular flows, or implementing drag forces formulations for polydisperse systems.

ACKNOWLEDGMENTS

We thank Frederic Dubois and Remy Mozul for their valuable technical advice on the simulations in LMGC90 and MIGFLOW. We thank the developer groups of MIGFLOW at Université Catholique de Louvain, especially Jonathan Lambrechts and Vincent Legat, and Université de Montpellier for their assistance, and enriching thoughts and discussion. We also acknowledge the support of the High-Performance Computing Platform MESO@LR. Moreover, we would like to thank the anonymous referees for their valuable and constructive comments. Finally, this work was partially funded by the Ecos Nord C19P01/63672, for scientific cooperation between France and Colombia.

APPENDIX: EQUATIONS

In this study we use a coarse-grained numerical model FEM-DEM [28]. For the fluid phase motion, the incompressible Navier-Stokes equations are solved and averaged using a weight function for considering the influence of particles on the fluid. The packing fraction ϕ is the weight variable that represents the fluid volume $\nu = 1 - \phi$ in the fluid mesh elements. The particle motion is solved with the nonsmooth contact dynamics approach (NSCD). In this method, perfectly rigid particles interact by volume exclusion and Coulomb friction [33,34]. The following are the equations solved in the FEM-DEM model as proposed in the original paper [28].

The conservation laws for the fluid phase are

$$\rho_{\mathrm{f}}\left(\frac{\partial \boldsymbol{u}}{\partial t} + \boldsymbol{\nabla}\cdot\frac{\boldsymbol{u}\boldsymbol{u}}{\nu}\right) = \boldsymbol{\nabla}\cdot[2\mu_{\mathrm{f}}\nu\boldsymbol{d}(\boldsymbol{u}) - p\boldsymbol{I}] + \boldsymbol{f} + \nu\rho_{\mathrm{f}}\boldsymbol{g}, \tag{A1}$$

$$\frac{\partial \nu}{\partial t} + \boldsymbol{\nabla}\cdot\boldsymbol{u} = 0, \tag{A2}$$

where $\boldsymbol{u} = \nu\boldsymbol{w}$ is the mean velocity of the fluid phase, p is the pressure, $\boldsymbol{f}$ is the force of the particle-fluid interaction, $\boldsymbol{I}$ the identity tensor, and $\boldsymbol{d}(\boldsymbol{u})$ is the rate of deformation tensor, computed as:

$$\boldsymbol{d}(\boldsymbol{u}) \triangleq \left(\boldsymbol{\nabla}\frac{\boldsymbol{u}}{\nu} + \left(\boldsymbol{\nabla}\frac{\boldsymbol{u}}{\nu}\right)^{T}\right). \tag{A3}$$

Both pressure p and fluid velocity $\boldsymbol{u}$ depend on the packing fraction that is computed every time step with the particles position.

The particles' motion results from their contact interaction, solved with NSCD, and the particle-fluid interaction. The velocity of a single grain i is computed with Newton second law of motion:

$$\frac{d}{dt}(m_i\boldsymbol{v}_i) = m_i\boldsymbol{g} - V_i\boldsymbol{\nabla}p|_{\boldsymbol{x}_i} - \boldsymbol{D}_i, \tag{A4}$$

where m, V, $\boldsymbol{x}$, and $\boldsymbol{v}$ are the mass, volume, position, and velocity of a single grain, respectively. The particle-fluid interaction force $\boldsymbol{f}$ [see Eq. (A1)] is represented by the combination of $V_i\boldsymbol{\nabla}p|_{\boldsymbol{x}_i}$ and the drag force $\boldsymbol{D}_i$. Note that for dry simulations, particle-fluid interaction forces are zero.

In our study, the solution is considered two-dimensional assuming the particles as disks of unitary depth and, as consequence, the drag force $\boldsymbol{D}_i$ is computed as:

$$\boldsymbol{D}_i = G(\nu|_{\boldsymbol{x}_i})C_d\ d_i\ \frac{\rho_{\mathrm{f}}}{2}\left\|\boldsymbol{v}_i - \frac{\boldsymbol{u}_i}{\nu}\right|_{\boldsymbol{x}_i}\left\|\left(\boldsymbol{v}_i - \frac{\boldsymbol{u}_i}{\nu}\right|_{\boldsymbol{x}_i}\right), \tag{A5}$$

where d is the diameter of a single particle and C_d is the drag coefficient computed as:

$$C_d = \left(0.63 + \frac{4.8}{\sqrt{\mathrm{Re}_i}}\right)^2, \tag{A6}$$

and the Reynolds number

$$\mathrm{Re}_i = \frac{\sqrt{2d}\,v|_{\boldsymbol{x}_i}}{\mu_\mathrm{f}}. \tag{A7}$$

The function $G(v|_{\boldsymbol{x}_i})$, that multiplies the drag force of a single particle, considers the effect that the surrounding particles have on the fluid-particle interaction [29].

$$G\left(v|_{x_i}\right) = v^{-1.8}|_{\boldsymbol{x}_i} \tag{A8}$$

More details of the nonsmooth contact dynamics approach can be found in Refs. [33–35] and an extensive description of FEM-DEM model for granular flows can be found in Ref. [28].

[1] G. D. Scott, Packing of spheres: Packing of equal spheres, Nature (London) **188**, 908 (1960).

[2] W. F. Oquendo-Patiño and N. Estrada, Densest arrangement of frictionless polydisperse sphere packings with a power-law grain size distribution, Granular Matter **22**, 75 (2020).

[3] S. Courrech du Pont, P. Gondret, B. Perrin, and M. Rabaud, Granular Avalanches in Fluids, Phys. Rev. Lett. **90**, 044301 (2003).

[4] M. Cabrera and N. Estrada, Granular column collapse: Analysis of grain-size effects, Phys. Rev. E **99**, 012905 (2019).

[5] E. Lajeunesse, J. B. Monnier, and G. M. Homsy, Granular slumping on a horizontal surface, Phys. Fluids **17**, 103302 (2005).

[6] N. J. Balmforth and R. R. Kerswell, Granular collapse in two dimensions, J. Fluid Mech. **538**, 399 (2005).

[7] C.-H. Lee, Z. Huang, and M.-L. Yu, Collapse of submerged granular columns in loose packing: Experiment and two-phase flow simulation, Phys. Fluids **30**, 123307 (2018).

[8] G. Pinzon and M. Cabrera, Planar collapse of a submerged granular column, Phys. Fluids **31**, 086603 (2019).

[9] A. Bougouin and L. Lacaze, Granular collapse in a fluid: Different flow regimes for an initially dense-packing, Phys. Rev. Fluids **3**, 064305 (2018).

[10] L. Staron and E. J. Hinch, Study of the collapse of granular columns using two-dimensional discrete-grain simulation, J. Fluid Mech. **545**, 1 (2005).

[11] V. Topin, Y. Monerie, F. Perales, and F. Radjaï, Collapse Dynamics and Runout of Dense Granular Materials in a Fluid, Phys. Rev. Lett. **109**, 188001 (2012).

[12] A. Busch and S. T. Johansen, On the validity of the two-fluid-ktgf approach for dense gravity-driven granular flows as implemented in ansys fluent r17.2, Powder Technol. **364**, 429 (2020).

[13] L. Jing, G. C. Yang, C. Y. Kwok, and Y. D. Sobral, Dynamics and scaling laws of underwater granular collapse with varying aspect ratios, Phys. Rev. E **98**, 042901 (2018).

[14] C. Meruane, A. Tamburrino, and O. Roche, On the role of the ambient fluid on gravitational granular flow dynamics, J. Fluid Mech. **648**, 381 (2010).

[15] Y.-h. Sun, W.-t. Zhang, X.-l. Wang, and Q.-q. Liu, Numerical study on immersed granular collapse in viscous regime by particle-scale simulation, Phys. Fluids **32**, 073313 (2020).

[16] G. C. Yang, L. Jing, C. Y. Kwok, and Y. D. Sobral, Pore-scale simulation of immersed granular collapse: Implications to submarine landslides, J. Geophys. Res.: Earth Surf. **125**, e2019JF005044 (2020).

[17] L. Staron and E. Hinch, The spreading of a granular mass: role of grain properties and initial conditions, Granular Mat. **9**, 205 (2007).

[18] M. Cabrera and N. Estrada, Is the grain size distribution a key parameter for explaining the long runout of granular avalanches? J. Geophys. Res.: Solid Earth **126**, e2021JB022589 (2021).

[19] N. Estrada, Effects of grain size distribution on the packing fraction and shear strength of frictionless disk packings, Phys. Rev. E **94**, 062903 (2016).

[20] E. Azéma, S. Linero, N. Estrada, and A. Lizcano, Shear strength and microstructure of polydisperse packings: The effect of size span and shape of particle-size distribution, Phys. Rev. E **96**, 022902 (2017).

[21] D. Cantor, E. Azéma, P. Sornay, and F. Radjai, Rheology and structure of polydisperse three-dimensional packings of spheres, Phys. Rev. E **98**, 052910 (2018).
[22] D. Cantor, E. Azéma, and I. Preechawuttipong, Microstructural analysis of sheared polydisperse polyhedral grains, Phys. Rev. E **101**, 062901 (2020).
[23] L. Amarsid, J.-Y. Delenne, P. Mutabaruka, Y. Monerie, F. Perales, and F. Radjai, Viscoinertial regime of immersed granular flows, Phys. Rev. E **96**, 012901 (2017).
[24] L. Rondon, O. Pouliquen, and P. Aussillous, Granular collapse in a fluid: Role of the initial volume fraction, Phys. Fluids **23**, 073301 (2011).
[25] L. Lacaze, J. Bouteloup, B. Fry, and E. Izard, Immersed granular collapse: from viscous to free-fall unsteady granular flows, J. Fluid Mech. **912**, A15 (2021).
[26] C. Meruane, A. Tamburrino, and O. Roche, Dynamics of dense granular flows of small-and-large-grain mixtures in an ambient fluid, Phys. Rev. E **86**, 026311 (2012).
[27] K. He, H. Shi, and X. Yu, An experimental study on aquatic collapses of bidisperse granular deposits, Phys. Fluids **33**, 103311 (2021).
[28] M. Constant, F. Dubois, J. Lambrechts, and V. Legat, Implementation of an unresolved stabilised fem–dem model to solve immersed granular flows, Comput. Part. Mech. **6**, 213 (2019).
[29] J. Richardson and W. Zaki, The sedimentation of a suspension of uniform spheres under conditions of viscous flow, Chem. Eng. Sci. **3**, 65 (1954).
[30] R. Beetstra, M. van der Hoef, and J. Kuipers, Numerical study of segregation using a new drag force correlation for polydisperse systems derived from lattice-boltzmann simulations, Chem. Eng. Sci. **62**, 246 (2007).
[31] F. Cello, A. Di Renzo, and F. P. Di Maio, A semi-empirical model for the drag force and fluid–particle interaction in polydisperse suspensions, Chem. Eng. Sci. **65**, 3128 (2010).
[32] C. Knight, C. O'Sullivan, B. van Wachem, and D. Dini, Computing drag and interactions between fluid and polydisperse particles in saturated granular materials, Comput. Geotech. **117**, 103210 (2020).
[33] J. J. Moreau, Sorne numerical methods in multibody dynamics: Application to granular materials, Eur. J. Mech. A. Solids **13**, 93 (1994).
[34] M. Jean, The non-smooth contact dynamics method, Comput. Methods Appl. Mech. Eng. **177**, 235 (1999).
[35] F. Dubois, V. Acary, and M. Jean, The contact dynamics method: A nonsmooth story, C. R. Mec. **346**, 247 (2018).
[36] LMGC90, available at https://git-xen.lmgc.univ-montp2.fr/lmgc90/lmgc90_user.
[37] MigFlow Project, available at https://git.immc.ucl.ac.be/fluidparticles/migflow.
[38] L. D. Dalcin, R. R. Paz, P. A. Kler, and A. Cosimo, Parallel distributed computing using python, Adv. Water Resour. **34**, 1124 (2011).
[39] K. Kumar, J.-Y. Delenne, and K. Soga, Mechanics of granular column collapse in fluid at varying slope angles, J. Hydrodyn. **29**, 529 (2017).
[40] J. Capecelatro and O. Desjardins, An euler–lagrange strategy for simulating particle-laden flows, J. Comput. Phys. **238**, 1 (2013).
[41] J. K. Mitchell, K. Soga *et al.*, *Fundamentals of Soil Behavior* (Wiley, New York, 2005), Vol. 3.
[42] E. L. Hinrichsen, J. Feder, and T. Jøssang, Random packing of disks in two dimensions, Phys. Rev. A **41**, 4199 (1990).
[43] H. Kausch, D. Fesko, and N. Tschoegl, The random packing of circles in a plane, J. Colloid Interface Sci. **37**, 603 (1971).
[44] See Supplemental Material at http://link.aps.org/supplemental/10.1103/PhysRevFluids.7.084304 for videos of column collapses at aspect ratios $a = [1.0, 3.5]$ and $\lambda = [1.2, 5, 19]$, for both dry and immersed conditions, for a table with the parameters of each simulation, and the data supporting the conclusions presented in this work.
[45] E. L. Thompson and H. E. Huppert, Granular column collapses: Further experimental results, J. Fluid Mech. **575**, 177 (2007).